BIOCHEMISTRY
including biophysical chemistry & molecular biology
Article

Biochemistry **2009,** *48,* 4273–4284 4273
DOI:10.1021/bi900290c

Cellular Copper Import by Nanocarrier Systems, Intracellular Availability, and Effects on Amyloid β Peptide Secretion[†]

Carina Treiber,[‡] Mohiuddin Abdul Quadir,[‡] Philipp Voigt,[§] Michal Radowski,[‡] Shangjie Xu,[‡] Lisa-Marie Munter,[‡] Thomas A. Bayer,[∥] Michael Schaefer,[§,⊥] Rainer Haag,[‡] and Gerd Multhaup*[,‡]

[‡]*Freie Universität Berlin, Institut für Chemie und Biochemie, Thielallee 63, D-14195 Berlin, Germany,* [§]*Molekulare Pharmakologie and Zellbiologie, Neurowissenschaftliches Forschungszentrum, Charité-Universitätsmedizin Berlin, D-14195 Berlin, Germany, and* [∥]*Department of Psychiatry and Psychotherapy, Universität Göttingen, Göttingen, Germany*[⊥] *Present address: Medizinische Fakultät der Universität Leipzig, Rudolf-Boehm-Institut für Pharmakologie und Toxikologie, 04107 Leipzig, Germany*

Received February 19, 2009; Revised Manuscript Received March 29, 2009

ABSTRACT: Studies in animals have reported that normalized or elevated Cu levels can inhibit or even remove Alzheimer's disease-related pathological plaques and exert a desirable amyloid-modifying effect. We tested engineered nanocarriers composed of diverse core−shell architectures to modulate Cu levels under physiological conditions through bypassing the cellular Cu uptake systems. Two different nanocarrier systems were able to transport Cu across the plasma membrane of yeast or higher eukaryotic cells, CS-NPs (core−shell nanoparticles) and CMS-NPs (core−multishell nanoparticles). Intracellular Cu levels could be increased up to 3-fold above normal with a sublethal dose of carriers. Both types of carriers released their bound guest molecules into the cytosolic compartment where they were accessible for the Cu-dependent enzyme SOD1. In particular, CS-NPs reduced Aβ levels and targeted intracellular organelles more efficiently than CMS-NPs. Fluorescently labeled CMS-NPs unraveled a cellular uptake mechanism, which depended on clathrin-mediated endocytosis in an energy-dependent manner. In contrast, the transport of CS-NPs was most likely driven by a concentration gradient. Overall, nanocarriers depending on the nature of the surrounding shell functioned by mediating import of Cu across cellular membranes, increased levels of bioavailable Cu, and affected Aβ turnover. Our studies illustrate that Cu-charged nanocarriers can achieve a reasonable metal ion specificity and represent an alternative to metal-complexing agents. The results demonstrate that carrier strategies have potential for the treatment of metal ion deficiency disorders.

Inherited disorders of Cu transport have illustrated the essential role of Cu in brain metabolism. Cu ions are cofactors of several metalloenzymes and are essential for central nervous system (CNS)[1] development (*1*). A disruption of Cu homeostasis during fetal life leads to perinatal mortality, severe growth retardation, and neurodegeneration (*2*). Mutations in Cu-transporting P-type ATPases ATP7A and ATP7B were shown to disrupt the homeostatic Cu balance resulting in CNS disease caused by Cu deficiency (Menkes disease) or Cu overload (Wilson disease) (*3*−*5*).

Aberrant metal homeostasis has also been implicated in Alzheimer's disease (AD), and a double-level molecular interaction has been proposed. First, Cu is known to bind the Aβ subunits of amyloid plaques (*6*, *7*). Second, the amyloid precursor protein (APP) (*8*), from which Aβ is released upon proteolytic cleavage (*9*), has a Cu-binding site in its large extracellular region (APP residues 124−189) (*10*). APP binds Cu(II) with nanomolar affinity (*10*) and reduces it to Cu(I) in vitro (*11*).

APP is actively involved in balancing Cu concentrations in the CNS. In APP knockout (KO) mice, Cu levels were found to be increased in the cerebral cortex (*12*), while transgenic overexpression of APP had opposite effects in cultured neurons and mice (*13*, *14*). APP was shown in yeast cells to have a Cu efflux activity (*15*), thereby explaining why APP-overexpressing mice exhibited the opposite effects and why these animals had a reduced SOD1 activity (*13*). In agreement with this, a genetically upregulated Cu level was associated with increased survival of APP transgenic mice prior to the detection of Aβ plaques formed by the human APP transgene (*16*).

Consequently, in a clinical trial, potential beneficial effects of oral intake of Cu(II)-orotate-dihydrate (8 mg of Cu daily) were investigated in AD patients. Although results demonstrated that oral Cu intake has neither a detrimental nor a promoting effect on the progression of AD (*17*), Cu treatment stabilized plasma

[†]This work was supported in part by the Deutsche Forschungsgemeinschaft (DFG), the BMBF, the International Copper Association (ICA), and the EC (QLK4-CT-2002-02723).

*To whom correspondence should be addressed: Freie Universität Berlin, Institut für Chemie und Biochemie, Thielallee 63, D-14195 Berlin, Germany. Phone: +49-30-838-555-33. Fax: +49-30-838-565-09. E-mail: multhaup@biochemie.fu-berlin.de.

[1]Abbreviations: Aβ, amyloid β-peptide; AD, Alzheimer's disease; APP, amyloid precursor protein; CNS, central nervous system; CMS-NPs, core−multishell nanoparticles; CQ, clioquinol; CS-NPs, core−shell nanoparticles; ICP-MS, inductively coupled plasma mass spectrometry; SOD1, superoxide dismutase 1.

© 2009 American Chemical Society
Published on Web 3/30/2009

and CSF levels in AD patients and antagonized the unbalanced Cu levels likely by activating the homeostatic system, i.e., by normalizing the uptake and excretion pathways (*17*). The clinical study revealed slightly stabilized Aβ levels, which serve as CSF biomarkers in AD patients (*17*). This is similar to an animal study in which raised brain Cu levels led to a decrease in amyloid plaque and plasma Aβ levels due to the expression of a mutant CuATPase7b (*16*). Conclusively, long-term intake of Cu can stabilize Cu levels in plasma and CSF of men, and the outcome of the clinical study is in line with findings obtained in APP-overexpressing mice where normal Cu levels and SOD1 activity could be restored by a dietary approach (*13*).

Recent studies with clioquinol (CQ), an 8-OH quinoline with a moderate affinity for Cu and Zn, the lipophilic chelator (DP109), isatin-Schiff base Cu(II) complexes, and metal bis(thiosemicarbazonato) complexes confirmed that promoting Cu uptake is a reasonable disease-modifying approach (*15*, *18*−*20*). This led us to investigate if engineered nanoparticles could be a superior alternative for addressing cellular Cu deficiency at the molecular level. Variants of these vehicles have been tested in clinical trials (*21*, *22*) on the basis of their drug solubilization and delivery ability (*23*).

Here, we identify functionalized nanocarriers consisting of hyperbranched poly(ethyleneimine) (PEI) as the core molecule surrounded by one (CS-NPs) or two (CMS-NPs) organic shells being able to encapsulate and to transport Cu into living cells. In our study, nanocarriers were selected according to their avidity for Cu. Both types of carriers approximately encapsulated a maximum of ~40 Cu(II) ions. Two specific nanocarriers of each group were characterized in detail for the transport of Cu across the plasma membrane. CS-NPs targeted intracellular organelles more efficiently than CMS-NPs. The cellular localization of CS-NPs directly correlated with the nature of the surrounding shell and qualified CS-NPs to affect extracellular Aβ levels in a dose-dependent manner. Whereas CMS-NPs were endocytosed in an energy-dependent manner, CS-NPs bypassed the cellular uptake system through diffusion along a concentration gradient.

EXPERIMENTAL PROCEDURES

Synthesis of CMS-NP and CS-NP Nanocarriers. Core−single-shell (CS) and core−multishell nanoparticles (CMS-NPs) were prepared by functionalizing hyperbranched PEI as the core molecule. In the case of CMS-NPs, the PEI core was functionalized by linear amphiphilic building blocks fromed by alkyl diacids connected to monomethyl poly(ethylene glycol) (mPEG with 6, 10, and 14 glycol units on average) (*24*). The standard esterification protocol was used under Dean−Stark conditions to attach the diacid to mPEG in the presence of *p*-toluenesulfonic acid (PTSA) as a catalyst. Activating the free carboxyl group of this amphiphilic building block as *N*-hydroxysuccinimide esters using dicyclohexyl carbodiimide (DCC) and *N*-hydroxysuccinimide (HONSu) followed by coupling to hyperbranched PEI yielded the desired product with a yield of 95−98%.

Of the two variants of CS-NPs, CS-Gly was synthesized by addition of DL-glycidol to a solution of PEI in methanol, resulting in a complete conversion of the reactive epoxide group after 24 h at room temperature. On the other hand, PEI, D-glucono-1,5-lactone, and a stoichiometric amount of water were mixed together at an elevated temperature (140 °C) for 10 min to give CS-Glu in 99% yield (*25*). Core−shell nanoparticles (CS-NPs) are surrounded by only one aminoglycerol shell (CS-Gly) or one gluconamide shell (CS-Glu). The PEI core of multishell nanoparticles (CMS-NPs) is enclosed by two shells (Figure 1). For an overview of the chemical composition of the carriers, see Table 1.

Fluorescent Labeling of CMS- and CS-NP Nanocarriers. Indocarbocyaninecarboxylic acid was dissolved in 10 mL of DMF, and the mixture was cooled to 0 °C. *N*-Hydroxysuccinimide (HOSu) and *N*,*N*′-dicyclohexylcarbodiimide (DCC) were added subsequently. After being stirred for 3 h, a solution of GS-Gly or CMS-2 in 2 mL of DMF was added dropwise. The resulting solution was stirred at room temperature overnight. The solvent was evaporated, and the crude product was dialyzed in methanol for 2 days to give the ICC-labeled nanocarriers. The loading degree of ICC was determined by UV−vis measurements.

Ultraviolet and Visible (UV−vis) Absorption Spectroscopy. Ultraviolet and visible absorption scans were taken using a Scinco S-3100 spectrophotometer in a quartz cell with a path length of 1 cm at room temperature based on a previously described protocol (*25*, *26*). Briefly, to assess the maximum metal cargo capacity of dendrimers and hyperbranched polymers, an aqueous solution of the individual nanotransporter (at various concentrations calculated according to the M_n value) was mixed with an aqueous solution of Cu(II) to yield a distinct molar [Cu(II) ions/nanotransporter] ratio within the range of 0−100. The solutions were incubated for 24 h at room temperature to reach equilibrium, a process assisted by uniform magnetic stirring.

Yeast Culture. *Pichia pastoris* cells were grown overnight in 30 mL of BMGY medium [1% (w/v) yeast extract, 2% (w/v) bactopeptone, 100 mM potassium phosphate (pH 6.0), 1.34% (w/v) yeast nitrogen base, 4×10^{-5}% biotin, and% (w/v) glycerol] followed by induction for 48 h in 75 mL of BMMY medium [BMGY with 2% (v/v) methanol instead of glycerol]. To investigate the effect of nanocarriers, the induction medium was adjusted to 10 μM with carrier or with carrier preloaded in a 1:1 stoichiometry (10 μM) with Cu(II)Cl_2.

For SOD activity measurements, 2×10^8 cells were harvested in the late exponential phase of growth and centrifuged at 3500 rpm for 10 min, resuspended in 1 mL of H_2O, washed once with 0.5 M EDTA (pH 8.0), and then resuspended again in 1 mL of H_2O. Washed cell pellets were resuspended in 100 μL of lysis buffer [50 mM potassium phosphate buffer (pH 7.4), 5% (v/v) glycerol, 45 mM $MgCl_2$, and 9×10^{-3} μg/μL DNase] with 5 μL of Complete (Roche) and an equal volume of acid-washed glass beads (0.5 mm, Sigma) followed by eight cycles of vortexing for 30 s and alternating cooling for 30 s on ice.

For metal ion determinations by ICP-MS, cells grown in 15 mL of culture were centrifuged and analyzed as described above.

SOD1 Assays. The assay for SOD1 activity was purchased from Dojindo and is based on the highly water-soluble tetrazolium salt, WST-1 [2-(4-iodophenyl)-3-(4-nitrophenyl)-5-(2,4-disulfophenyl)-2*H*-tetrazolium, monosodium salt], that produces a water-soluble formazan dye upon reduction with a superoxide anion. The rate of reduction of superoxide anion is linearly related to the xanthine oxidase (XO) activity and is inhibited by SOD1. The absorbance can be measured at 450 nm. Sample preparation for the SOD1 activity assay (Dojindo) was conducted as described above but with samples diluted 1:5. Assays were performed according to the manufacturer's instructions. Western blot analysis was applied using a polyclonal SOD1 antibody (Natutec, Frankfurt, Germany).

Inductively Coupled Plasma Mass Spectrometry (ICP-MS). To determine the metal ion content of washed cell pellets,

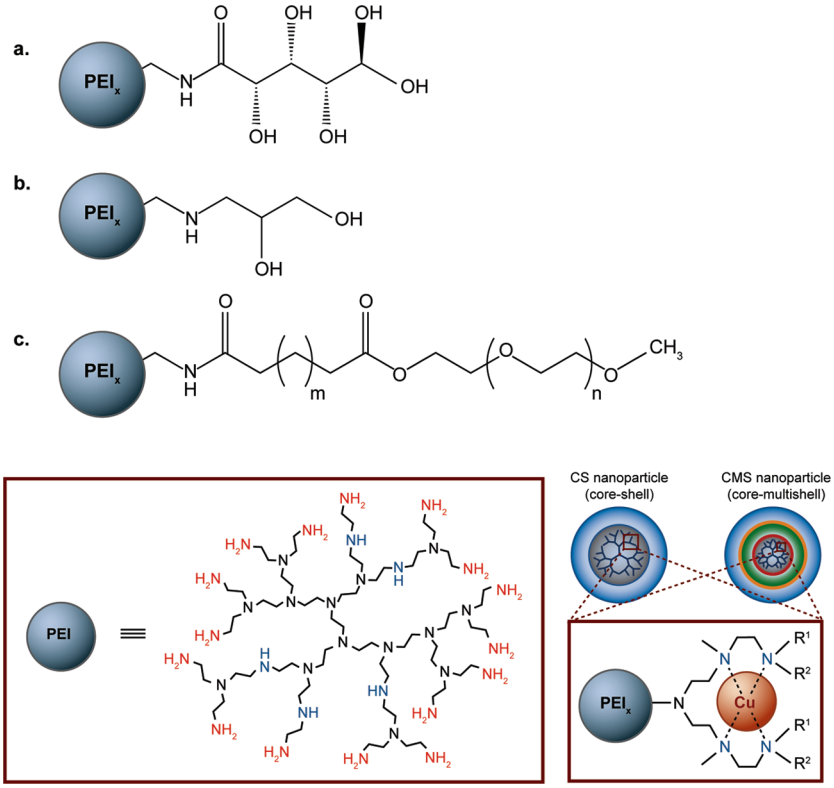

FIGURE 1: Architecture of CMS-NPs (core−multishell nanoparticles) and CS-NPs (core−shell nanoparticles). CS-NPs with either glycidol or gluconolactone and CMS-NPs with a double-layered envelope. PEI molecules of CMS-NPs are functionalized with linear amphiphilic diacid alkyl chains linked to poly(ethylene glycol) monomethyl esters: (a) CS-Glu, $x = 10$ kDa; (b) CS-Gly, $x = 10$ kDa; and (c) CMS systems, $x = 3.6$ kDa, $m = 18$, and $n = 10$ for CMS-1, and $x = 10$ kDa, $m = 18$, and $n = 6$ for CMS-2. In the bottom panel, the schematic concept of CS and CMS nanoparticles with the PEI core is illustrated; the proposed Cu coordination within the NPs is shown [in the case of functionalization of primary amine groups of the PEI core, $R^1 = R^2$ = glycidol or gluconolactone adducts for CS-NPs and linear diacid alkyl chains linked to poly(ethylene glycol) monomethyl esters for CMS-NPs, while for secondary amine functionalization, R^1 = H]. CryoTEM measurements revealed the CMS-NPs with a diameter range of 4−6 nm coexist with larger spherical aggregates of 30−50 nm when the critical assembly concentration of 0.1 g/L is reached (*24*). For the core−single-shell particles, unimers in the range of 5 nm are also found at low concentrations while at high concentrations aggregation is also observed (*25*, *54*).

Table 1: Chemical Composition of Nanocarriers

	core	core M_n[a] (g mol^{-1})	no. of shells	shell 1	shell 2	nanotransporter M_n[a] (g mol^{-1})	DF[b] (%)	N[c] (mmol/g of polymer)
CS-Glu	PEI	10000	1	gluconolactone	−	23000	55	3.33
CS-Gly	PEI	10000	1	glycidol	−	18400	30	6.46
CMS-1	PEI	3600	2	C18 alkyl	PEG 10	22000	42	1.45
CMS-2	PEI	10000	2	C18 alkyl	PEG 6	42000	32	2.75

[a] Average molecular weight. [b] Degree of functionalization with respect to terminal and linear amine groups. [c] Numbers of amino groups in millimoles with respect to terminal and linear amino groups per gram of polymer.

ICP-MS was performed by using a HP4500 Series 300 Shield-Torch system instrument (Agilent, Waldbronn, Germany) in peak hopping mode with a spacing at 0.05 atomic mass unit, three points per peak, three scans per replicate, and an integration time of 300 ms per point as described previously (*27*). The rate of plasma flow was 15 L/min with an auxiliary flow of 0.9 L/min and a blend gas flow rate of 0.1 L/min. The RF power was 1.2 kW. The sample was introduced using a crossflow nebulizer at a flow rate of 1.02 L/min. The apparatus was calibrated with a 6.5% HNO_3 solution containing Cu and Zn at 1, 5, 10, 25, 50, 100, 200, and 400 ppb with ^{103}Rh as the internal standard for all isotopes. To compare the determined intracellular amount of metal ion per cell, data were normalized by the amount of cells. Samples were measured three times, and statistical analysis was performed using three independent measurements by calculating the standard error of the mean (SEM). Statistical significance was determined by the Student's t test.

Cell Culture. Wild-type Chinese hamster ovary (CHO) cells, a human neuroblastoma SH-SY5Y cell line, a human hepatocellular carcinoma cell line (Hep G2), and human embryonic kidney (HEK293) cells were cultured as described previously (www.lgcpromochem-atcc.com). Cells at a density of 10500 cells/cm^2 were used at the time of the experiment from either cell line. This allowed differentiation between toxic activities of carriers (Table 2) and toxic activities against individual cell lines that vary in their individual Cu content. Stock solutions of nanoparticles with Cu were prepared in Milli-Q water by thorough mixing.

For toxicity assays, higher eukaryotic cell lines were incubated for 5 h with different concentrations of Cu-saturated nanoparticles; e.g., experiments in SH-SY5Y cells were carried out using a nanotransporter at a concentration of 30 nM, which is one-sixth of the measured LD_{50} values.

Sandwich ELISA. Stably APP transfected SH-SY5Y cells (*28*) were plated at a density of 2.8×10^5 cells/12-well dish. Cells

were treated in OptiMEM medium (Invitrogen, Karlsruhe, Germany) supplemented with either $CuCl_2$ concentrations as indicated, vehicle control (PBS), or nanocarriers for 4 days. Aliquots of 200 μL of medium were directly assayed in triplicate with Aβ40- and Aβ42-specific ELISAs according to the manufacturer's instruction (The Genetics Company, TGC Zuerich).

Cell Lysis. Cells were washed with 1× PBS, scraped from the culture plates, and treated for 30 min at 4 °C in an end-over-end rotation device with lysis buffer [50 mM Tris-HCl (pH 7.5), 150 mM NaCl, 2% Triton X-100, and 2% NP40]. After lysis, cell debris was separated by centrifugation for 10 min at 10000 rpm and 4 °C, and supernatants were collected for further experiments.

MTT Assays. MTT assays were purchased from Promega (Mannheim, Germany) and performed in 96-well plates. This assay is based on tetrazolium salt 3-(4,5-dimethylthiazol-2-yl)-2,5-diphenyltetrazolium bromide (MTT) that is taken up into cells and reduced to yield a purple formazan product, which is largely impermeable to cell membranes, thus resulting in its accumulation within healthy cells. The number of cells of the different lines was normalized, and cells were cultured in 96-well plates, incubated for 48 h, and washed three times in 1× PBS (137 mM NaCl, 2.7 mM KCl, 10 mM Na_2HPO_4, and 2 mM KH_2PO_4) followed by treatment with OptiMEM medium (Invitrogen) supplemented with individual carrier in the absence (control) or presence of Cu for 5 h. The volume of tissue culture medium in each well was 100 μL, to which 20 μL of CellTiter 96 AQ_{ueous} One Solution Reagent was added. Plates were incubated for 1−4 h at 37 °C in a humidified, 5% CO_2 atmosphere. Then the absorbance was measured at 450 nm.

Subcellular Fractionation. SH-SY5Y cells were grown in 10 mm dishes to a density of 1.8×10^6 cells/well, washed three times with 1× PBS (137 mM NaCl, 2.7 mM KCl, 10 mM Na_2HPO_4, and 2 mM KH_2PO_4) followed by treatment with individual carriers in the presence and absence of added Cu for 5 h in OptiMEM medium (Invitrogen). The cell culture supernatant was collected and stored for ICP-MS analysis to determine Cu content. Cells were washed once in 1× PBS and scraped from the plates. A solution of 2 mL of 1× PBS and 0.1% Tween 20 was added to cells. After incubation for 10 min at 4 °C, lysis was performed by Dounce homogenization. Cells were centrifuged for 15 min at 500*g*, yielding P1 (nuclei and cytoskeleton), followed by a second centrifugation step at 2600*g* for 15 min, resulting in P2 (mitochondria, lysosomes, and peroxisomes). A final centrifugation was performed at 100000*g* for 30 min, resulting in P3 (plasma membrane, ER fragments, small vesicles, and microsomal fraction) and the respective supernatant (cytosol). P1, P2, P3, and supernatants were subjected to ICP-MS to determine the metal ion content of specific compartments. Western blot analysis was applied to verify purity of fractions as described previously (*15*). Dynamin was used as a cytosolic marker, frataxin for mitochondria, actin for cytoskeleton, histone for nuclei, and calnexin as a marker for the endoplasmic reticulum. All antibodies were purchased from Chemicon (Hampshire, U.K.).

Isolation of Nuclei. Cell pellets were obtained as described above. After being washed in 1× PBS, nuclei were prepared with the EZ PrepTM nucleus isolation kit (Sigma, Munich, Germany) for small-scale preparation of functional nuclei from mammalian cells. Briefly, cells were washed with 1× PBS, treated with 1 mL of Nuclei EZ lysis buffer (Sigma), and scraped from the dishes. Supernatants resulting from centrifugation at 500*g* contained cytoplasmic components. The pellet was resuspended in 700 μL of Nuclei EZ lysis buffer (Sigma) by vortexing followed by an incubation for 5 min on ice. The centrifugation step was repeated, and nuclei, as well as supernatant fractions, were separated before the metal ion content was determined by ICP-MS.

Isolation of Mitochondria. Cells were obtained as described above and then washed with 1× PBS. Cells were then scraped off from the dishes and treated for 2 min on ice with 0.8 mL of reagent A of a mitochondrion isolation kit (Pierce, Bonn, Germany). Cells were homogenized for 3 min with a Dounce glass homogenizer, before 0.8 mL of reagent C was added followed by centrifugation for 10 min at 4 °C and 700*g*, yielding cytosol and mitochondria in the supernatant. The supernatant was transferred to a new reaction tube and centrifuged again for 15 min at 4 °C and 3000*g*. Mitochondria and supernatant fractions were frozen before the metal ion content was determined by ICP-MS.

Confocal Laser-Scanning Microscopy (CLSM). Uptake of ICC-conjugated carriers was monitored by confocal microscopy on a LSM-510 META microscope equipped with a Plan-Apochromat 63×/1.4 objective (both Carl Zeiss). ICC was excited with the 543 nm laser line of a helium−neon laser using a 488/543 nm dichroic mirror. Signals were passed through a 560 nm long pass filter for detection. Pinholes were adjusted to yield optical sections of 1−1.2 μm. Cells were incubated on a heated stage in a buffer containing 10 mM HEPES (pH 7.4), 128 mM NaCl, 6 mM KCl, 1 mM $MgCl_2$, 1 mM $CaCl_2$, 5.5 mM glucose, and 0.2% bovine serum albumin.

RESULTS

Cu Encapsulation by Nanocarriers. Studies were performed to establish a novel nanocarrier system for transporting specifically Cu across cell membranes. The respective chemical composition of the material was optimized for the transport activity in yeast cells. The yeast growth medium was supplemented with precharged nanotransporters, and intracellular Cu concentrations were determined by ICP-MS analysis as described previously (*15*).

The nanoparticles were composed of poly(ethyleneimine) (PEI) differing in the structure of the shells. Core−shell nanoparticles (CS-NPs) were surrounded by only one amino glycerol shell (CS-Gly) or one gluconamide shell (CS-Glu), and multishell nanoparticles (CMS-NPs) functionalized with linear amphiphilic molecules were built from diacid alkyl chains. These are connected to poly(ethylene glycol) monomethyl ester via ester bonds and are thereby enclosed by two shells (Figure 1). Accordingly, two nanotransporters of the CMS-NP group, CMS-1 and CMS-2 (CMS-1 is $C_{3.6}MS_{PEG10}$; CMS-2 is $C_{10}MS_{PEG6}$), and two of the CS-NP group, CS-Glu and CS-Gly (Table 1), were further analyzed for the spontaneous encapsulation and their specific transport of metal ions. Nanocarriers were selected according to their avidity for Cu. Both types of carriers approximately encapsulated a maximum of ~40 Cu(II) ions per molecule as determined by UV−vis spectroscopic titration and ITC measurements (data not shown).

To test if nanocarriers can encapsulate endogenous Cu [the normal Cu concentration in medium is 0.5 μM (*15*)] or other divalent metal ions present in normal growth medium, methylotrophic yeast *P. pastoris* cells were incubated with individual molecules.

ICP-MS analyses of cell lysates revealed a carrier-facilitated cellular increase in the level of Cu for CMS-2, CS-Glu, CMS-1,

Table 2: LD_{50} Values (μM) of Free Cu or Cu-Saturated Nanocarriers for Individual Cell Lines

	Cu	CMS-1	CMS-2	CS-Glu	CS-Gly
CHO	40	1.2	2.5	1.8	0.5
HepG2	> 200	5.0	6.0	4.0	1.5
HEK293	6.0	1.0	0.8	0.5	0.6
SY5Y	10	1.5	1.5	0.4	0.2

and CS-Gly (Figure 2 A). This effect was specific for Cu, because carrier treatment did not increase Mn or Zn levels (Figure 2 B,C) with one exception. There was an ~10% increase in cellular Zn levels upon CS-Glu treatment, which is not observed when yeast cells were grown in medium supplemented with Cu-charged CS-Glu (see below). A slight reduction in the Mn level was caused by CMS-2 (Figure 2 B), and significantly decreased Zn levels were observed after treatment with CMS-2 and CS-Gly (Figure 2 C). This may be explained by the noninternalized nanocarriers encapsulating divalent metal ions from the normal medium and reducing the availability of the respective metal ion for the normal cellular transport system.

Cu uptake was further evaluated in yeast cells grown in medium supplemented with precharged nanocarriers (Figure 3). The slight increase in intracellular Cu level observed after incubation with uncharged carriers (Figure 2 A) could be significantly increased in the presence of preloaded carriers (Figure 3 A). The carrier-caused deviations in Zn and Mn levels became negligible under these conditions (Figure 3 B,C), except for a small but significant reduction of the Zn level by CS-Gly. Taken together, the supplementation of the medium with nanocarriers precharged with Cu yielded not only an additional increase in cellular Cu levels but also an increased specificity for the transport of Cu.

Accessibility of Carrier Cargo. In a previous study, we established *P. pastoris* lines that secrete the ectodomain of APP comprising amino acid residues 18−350, thereby proving Cu efflux activities of APP (*15*). To gain insight into a possible interference of Cu-charged nanocarriers with normal Cu acquisition mechanisms in yeast cells, we measured Cu levels in wild-type and in sAPP-expressing yeast cells.

Under normal growth conditions, Cu efflux activities of sAPP (*15*) fully antagonized the nanocarrier-mediated cellular Cu increase (Figure 4 A). sAPP-mediated Cu efflux activities could balance the Cu import of CMS-1 or CS-Glu carriers in medium supplemented with Cu-charged nanocarriers (Figure 4 B). The data show that carrier-imported Cu ions were accessible for sAPP-mediated export of all carrier-treated samples, which is evident from the differences in Cu levels between mock and sAPP-expressing cells (Figure 4 B). Strikingly, CS-Glu carriers are especially successful in Cu import and readily release their cargo into the cell for sAPP-mediated efflux.

We also determined the activity of cellular SOD in these yeast cells by using a quantitative SOD assay (*15*, *29*). The active enzyme SOD1 holoprotein, which also exists in a metal-free apo form, binds Cu and can thus serve as an established marker for Cu bioavailability (*30*). In agreement with previous studies using CQ−Cu complexes, treatment with all Cu-loaded carriers yielded an increase in SOD1 activity (Figure 5 A) that is not due to altered SOD1 protein levels as shown by Western blot analysis (Figure 5 B). Therefore, we conclude that Cu imported by precharged nanocarriers is in an exchangeable form and may therefore be available also for Cu-dependent enzymes other than

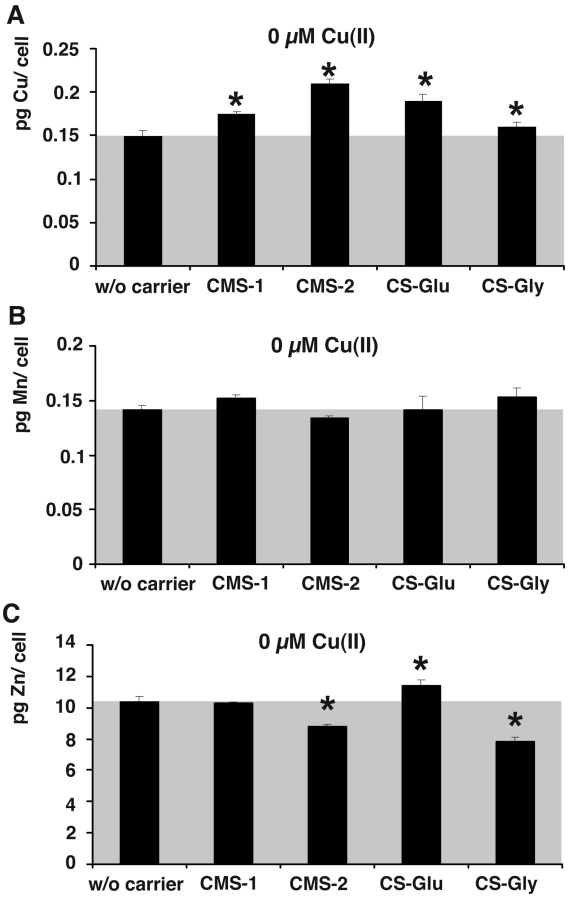

FIGURE 2: Nanocarrier treatment specifically increases intracellular Cu levels. Yeast cells were grown for 48 h in BMMY medium in the absence or presence of 10 μM nanocarriers added to the same cell density. Cell pellets of a 15 mL yeast culture were washed with EDTA, and the Cu, Mn, and Zn levels were determined by ICP-MS. (A) The intracellular Cu concentration is increased upon carrier treatment: 7% for CS-Gly, 16.8% for CMS-1, 27.5% for CS-Glu, and 40% for CMS-2. (B) Intracellular Mn concentrations are decreased but not significantly. (C) CS-Glu increased the intracellular Zn concentration up to 10%, while CMS-2 and CS-Gly decreased Zn levels by ~10 and ~20%, respectively. Differences in intracellular metal ion concentration were statistically significant with $p < 0.01$ (*) compared to untreated cells. Results were obtained from two to four independent samples and are expressed as the mean ± standard deviation of three measurements.

SOD1. Note that the increase in SOD activity does not correlate well with the increase in the intracellular Cu level (see Figure 3 A). While cytosolic SOD activity does not differ significantly among CS-Gly, CS-Glu, and CMS-2, it is highest for CMS-1 (Figure 5 A). This is seemingly in contrast to the Cu uptake data (Figure 4B) and leads us to conclude that (i) CMS-1 may easily release its bound guest molecules in the cytosolic compartment where they are accessible for Cu-dependent enzymes like SOD1 and (ii) other carriers analyzed may target different cellular compartments with their cargo.

Toxicity of Nanocarriers in Higher Eukaryotic Cells. The toxicity of Cu-loaded and of uncharged nanocarriers in higher eukaryotic cells was analyzed by the MTT assay. The LD_{50} values of individual nanotransporters were determined in the absence of Cu as a cargo in four different cell lines, i.e., Chinese hamster ovary (CHO), human hepatocellular liver carcinoma (Hep G2), human embryonic kidney (HEK 293), and human neuroblastoma (SH-SY5Y) (Table 2). The toxicity of carriers was observed at micromolar concentrations in a manner

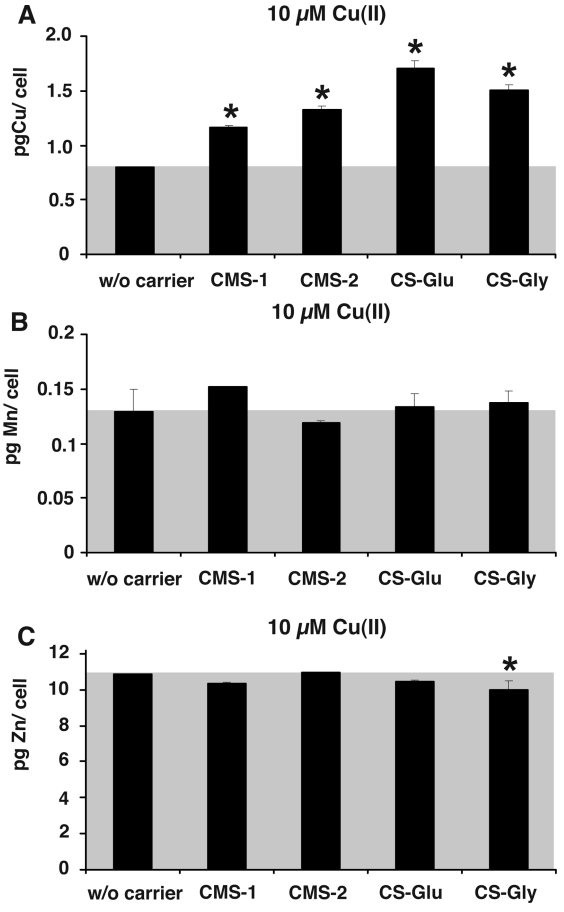

FIGURE 3: Nanocarriers preincubated with Cu at a 1:1 stoichiometry (10 μM) before addition to the growth medium specifically increase the intracellular Cu levels of yeast cells. (A) ICP-MS measurements revealed an increase in the intracellular Cu level of 50% for CMS-1, 107% for CS-Glu, 92% for CS-Gly, and 64% for CMS-2 in comparison to yeast cells grown in medium supplemented with Cu without nanocarriers. (B) Intracellular Mn levels are not significantly affected by the Cu-loaded nanoparticles. (C) Intracellular Zn levels are not significantly changed by treatment with Cu-loaded carriers except for CS-Gly which shows a slight decrease. Differences in intracellular metal ion concentration were statistically significant with $p < 0.01$ (*) compared to untreated cells. Values were obtained from two to four independent samples and are expressed as the mean ± standard deviation of three measurements.

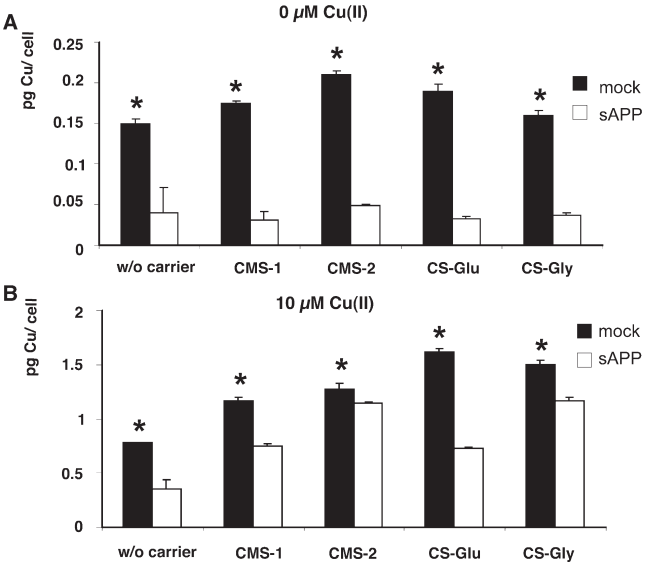

FIGURE 4: Nanocarriers precharged with Cu as described in the legend of Figure 3 partially antagonize the Cu efflux activity of APP in yeast cells. (A). ICP-MS measurements revealed that uncharged nanocarriers have no effects in sAPP-expressing yeast cells compared to mock-transfected cells where sAPP expression decreased intracellular Cu levels by 40%. Note that for easier comparison the same data that are shown in Figure 2 A (black bars) are included. (B) Intracellular Cu levels of cells grown in Cu-supplemented medium were balanced to normal levels of mock-transfected cells by CMS-1 and CS-Glu carriers. In CS-Glu-treated cells, sAPP-mediated Cu efflux activity reduced intracelluar Cu levels by 50%, indicating the accessibility of carrier-imported cargo for sAPP. Differences in intracellular metal ion concentration were statistically significant with $p < 0.01$ (*) compared to untreated cells. All decreases in sAPP-expressing cells vs the mock-transfected cells were statistically significant, i.e., without carrier ($p < 0.002$), with CMS-1 ($p < 0.0015$), with CMS-2 ($p < 0.01$), with CS-Glu ($p < 0.00004$), and with CS-Gly ($p < 0.004$). Note that for easier comparison the same data that are shown in Figure 3 A (black bars) are included. Values were obtained from two to four independent samples and are expressed as the mean ± standard deviation of three measurements.

independent of whether uncharged [data identical to those of Cu-charged particles (not shown)] or Cu-charged particles were tested (Table 2). Thus, nanocarriers per se were more toxic compared to the respective free Cu concentration, i.e., the cargo administered illustrating the negligible toxicity of the Cu cargo for the living cells.

The toxicity of Cu-charged nanocarriers could be ranked in decreasing order: CS-Gly > CS-Glu > CMS-NPs. This was most obvious in CHO and Hep G2 cells where the toxicity of CS-Glu was 3.6- and 2.6-fold higher than that of CS-Gly, respectively. SH-SY5Y neuroblastoma cells were most sensitive to Cu-charged nanocarriers, possibly due to a relatively low demand of brain cells for Cu compared to other cell lines tested. Hep G2 liver cells were most resistant to free Cu, which may correlate with the fact that the liver is the organ with the highest Cu concentration because the major Cu excretion route is through the bile. The LD_{50} values revealed that the shielding of the core structure by the surrounding shells determines the toxicity of the carriers. CMS-NP carriers were less toxic than CS-Gly and CS-Glu. This denounces PEI as a potential toxic factor since the better the shielding, the less toxic the carriers for living cells. Intracellular Cu levels could be increased upon Cu-charged carrier treatment between 1.5-fold (CS-NPs) and 3-fold above normal with a sublethal dose (25% of the carrier-specific LD_{50}). According to this proof-of-principle experiment, it may be possible to rescue Cu depletion in vivo more efficiently than shown before with a dietary approach using Cu sulfate (*13*).

Cellular Localization of Cu, Possible Target Compartments for the Carrier Cargo, and Effect on Aβ Production. As the data above indicated that these nanocarriers can enter cells and may have a specific cellular target for their cargo, we have assessed the cellular target compartments and the entry mechanisms for the different Cu-charged carriers. Therefore, SH-SY5Y cells were treated with free Cu or Cu-charged nanocarriers and fractionated by centrifugation. This yielded four subcellular fractions enriched in (i) nuclei, (ii) mitochondria, lysosomes, and peroxisomes, (iii) plasma membrane, ER fragments, small vesicles, and microsomal components, and (iv) the cytosol as revealed by Western blot analysis with specific antibodies recognizing marker proteins of the different cellular compartments. ICP-MS analysis of fractions revealed that the treatment with Cu-loaded nanocarriers specifically increased intracellular Cu levels in different compartments of SH-SY5Y cells (Figure 6) and of three other cell lines analyzed, whereas Cu levels were below the detection limit in fractions of untreated cells (data not

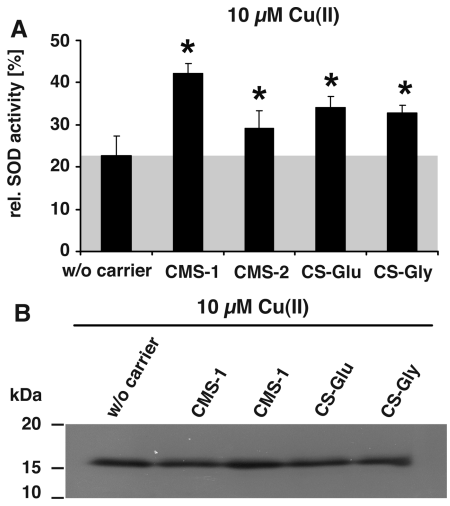

FIGURE 5: Carrier-mediated import of Cu increases total SOD activity at unchanged SOD1 protein levels. The SOD assay is based on the highly water-soluble tetrazolium salt WST-1 that produces a water-soluble formazan dye upon reduction with a superoxide anion. The rate of reduction of superoxide anion is linearly related to the xanthine oxidase (XO) activity. Activity is reported as relative units. (A). Supplementation of growth medium with Cu-loaded nanoparticles led to a statistically significant increase in SOD1 activity for the CMS-NP and CS-NP nanocarriers at $p < 0.01$ (*). (B) Western blot analysis in the presence of non-Cu-loaded (0 μM Cu) and Cu-loaded (10 μM Cu) nanoparticles does not show changes in SOD1 protein levels upon carrier treatment. Protein amounts loaded were standardized according to the cell number; samples were separated on 12% SDS gels, and SOD1 was detected with the polyclonal SOD1 antibody.

shown). Approximately ~40% of the total cellular Cu was found associated with membranes when cells were treated with Cu-preloaded CMS-NP carriers (40 Cu ions/carrier molecule) or with free Cu as indicated (Figure 6 A). The cargo of CS-NPs was favorably detected in the nuclear, mitochondrial, lysosomal, and peroxisomal fractions (Figure 6 B,C), whereas CMS-NPs were targeted to the cytosol (Figure 6 D). The purity of the different fractions was confirmed by Western blot analyses of compartment-specific marker proteins (Figure 6 E). Taken together, the results imply that Cu ions have reached cellular compartments by carrier-mediated transport.

We examined whether NPs also affected Aβ levels by measuring extracellular Aβ40 and -42 levels in the cell culture medium of treated cells (*28*). Only treatment with sublethal concentrations of free Cu (Table 2) or Cu-charged CS-Glu carriers had significant effects on Aβ40 and Aβ42 levels (Figure 6 F−I). All other carriers tested yielded inconsistent results (data not shown) probably due to the finding that CS-Glu carriers are especially efficient in Cu import and ready to release their cargo into the cell for the sAPP-mediated efflux (see above). The reduction of secreted Aβ in the culture medium of SH-SY5Y cells thus confirmed our previous studies with APP-expressing CHO cells where maximal inhibition of Aβ production was achieved in CHO-K1 cells at ~10 μM Cu (*31*). Taken together, both types of nanocarriers tested, CMS-NPs and CS-NPs, were able to mediate transport of Cu across plasma membranes with CS-NPs being more prone to target specific intracellular sites.

To further dissect the targeting specificity of the CS-NPs, we used purification kits to separate nuclei from the cytosol and to separate mitochondria from lysosomes and peroxisomes. ICP-MS analysis revealed that CS-Gly nanocarrier treatment led to a strong accumulation of Cu in the nuclei (Figure 7 A). Cu levels were 44-fold increased in P1 fractions of nuclei after CS-Gly treatment compared to incubation with free Cu (Figure 7 A). Cu levels were 3-fold increased compared to that of CS-Glu treatment, whereas CMS-NP carriers were much less efficient (Figure 7 A). Note that the inserted graph in Figure 7A illustrates that the composition of the respective polymer can directly influence the nuclear Cu content. The purity of nuclear fractions was analyzed by Western blot analysis using antibodies against marker proteins (Figure 7 B). ICP-MS analysis of isolated mitochondria (Figure 7 C) revealed that CS-NPs preferentially increased Cu levels in mitochondria. CS-Glu increased Cu levels up to 29-fold compared to cells treated with free Cu. The purity of mitochondria fractions was analyzed by Western blot analysis using antibodies against marker proteins (Figure 7 D). The CMS-NPs were less specific for targeting mitochondria since the increase in Cu levels was similar to that with free Cu treatment. Taken together, CS-Glu preferentially led to an accumulation of Cu in mitochondria compared to CS-Gly that strongly increased Cu levels in the nuclei.

Endocytosis of CMS-NPs and CS-NPs. To investigate how nanocarriers can cross cellular membranes, carriers were covalently modified with the fluorescent dye indocarbocyanine (ICC). The internalization of carriers by living cells was followed by confocal laser-scanning microscopy. ICC-labeled CMS-NPs were observed in vesicle-like structures after incubation for 20 min (Figure 8 A, left panel). Exposure of cells to hypertonic medium inhibited the transport of CMS-NPs across cellular membranes (Figure 8 A, right panel), indicating that endocytosis was mediated via the clathrin-coated pit pathway in SH-SY5Y cells. In contrast to CMS-NPs, ICC-labeled CS-NPs could not be detected in vesicular structures. After incubation for 20 min, ICC-labeled CS-NPs were found in the cytosol but also in nuclear compartments (Figure 8 B, left panel). Since hypertonic medium did not inhibit intracellular localization (Figure 8 B, right panel) and trypan blue staining indicated that cells were viable (data not shown), we can only speculate about the mechanism of how CS-NPs were taken up. Most likely, highly positively charged CS-NPs first adhere to the plasma membrane before a transport across the membrane occurs, which is driven by the concentration gradient. This is in agreement with the finding that inhibitors of endocytosis did not affect intracellular Cu concentrations modulated by CS-NPs as analyzed by ICP-MS measurements (Figure 8 C). An inhibition of clathrin-dependent, receptor-mediated endocytosis of Cu-charged CMS-NPs by hyperosmolar sucrose or the presence of chlorpromazine reduced the intracellular Cu concentration by 95% compared with the control, i.e., in the absence of inhibitors (Figure 8 C). Likewise, filipin treatment, which is known to disrupt caveolae and caveolae-like structures, led to a 70% reduction (Figure 8 C), and sodium azide that inhibits cellular respiration reduced the rate of uptake of Cu by 84% (Figure 8 C). In contrast to CS-NPs, CMS-NPs were most likely endocytosed via a clathrin-mediated pathway and in an energy-dependent manner. Nevertheless, both types of hyperbranched nanotransporters could mediate cellular import of Cu ions by bypassing the normal cellular Cu transport machinery.

DISCUSSION

Recent studies have focused on the role of Cu in the pathogenesis of AD, including Cu supplementation treatments of affected patients based on animal studies and cell culture system analyses. Administering Cu has been found to stimulate the

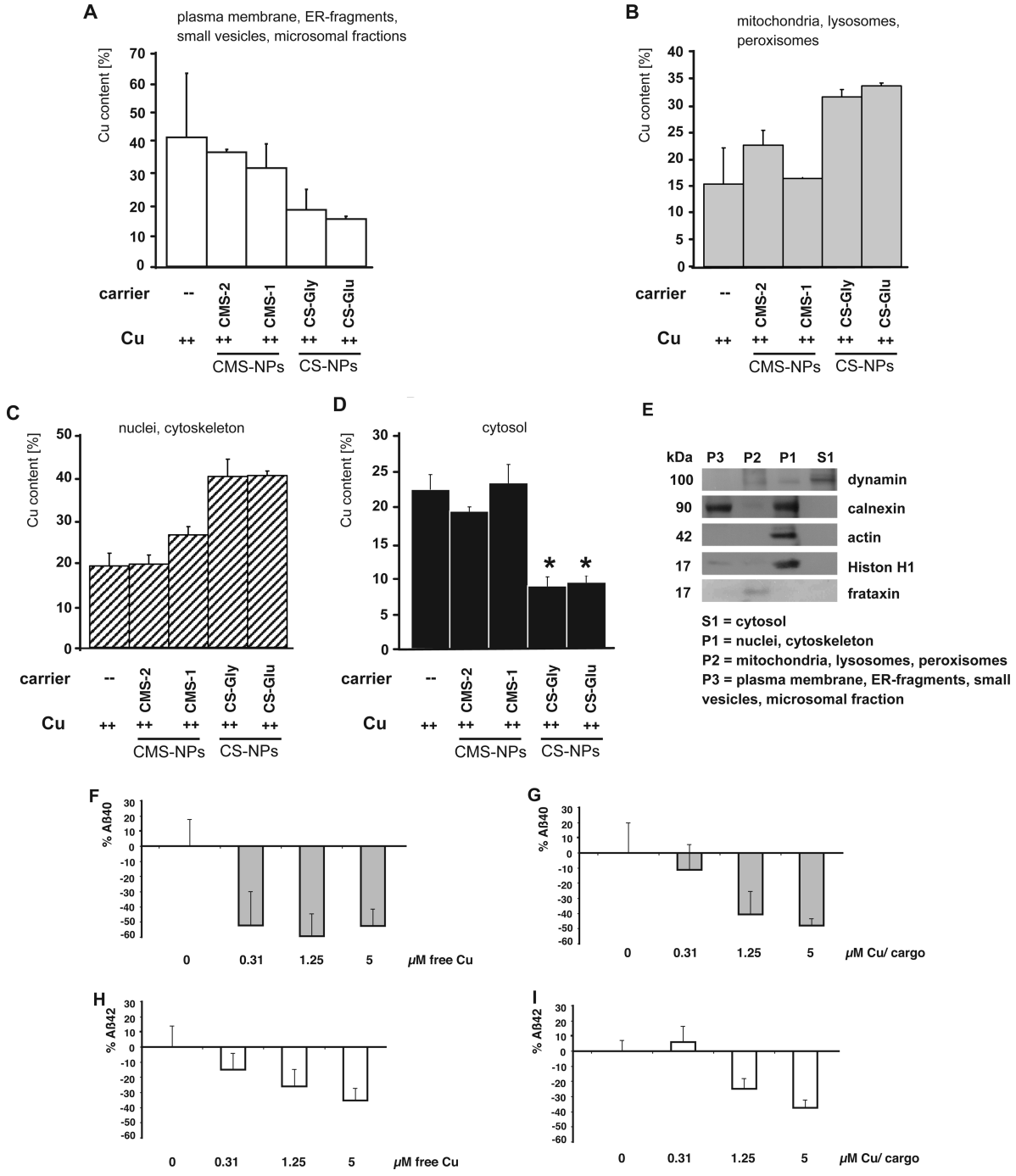

FIGURE 6: Cu-charged nanoparticles target intracellular compartments. SH-SY5Y cells were treated with 30 nM nanoparticles that were saturated with Cu for 5 h, washed with PBS, and fractionated by several centrifugation steps. (A). Cu content in fraction 1 containing plasma membrane, ER fragments, small vesicles, and microsomal components as determined by ICP-MS. (B) Cu content in fraction 2 containing mitochondria, lysosomes, and peroxisomes. (C) Cu content in fraction 3 containing nuclei and cytoskeleton. (D) Cu content in fraction 4 containing cytosolic components. CS-NPs preferentially target intracellular organelles compared with CMS-NPs ($p < 0.001$). Bars represent the relative Cu content since Cu levels determined in fractions of untreated cells were subtracted as background from those cells treated with nanocarriers alone or from cells treated with free Cu. (E) Purity of different fractions confirmed by Western blot analysis. Protein amounts loaded were standardized to 20 μg of total protein as determined by the BCA assay. Proteins were separated on a 12% polyacrylamide−SDS gel, and organelle marker proteins were detected using specific monoclonal antibodies as indicated. (F−I) Reduction of secreted Aβ levels of APP-SH-SY5Y cell cultures treated with free Cu (F and H) or Cu-charged CS-Glu (G and I) at Cu cargo concentrations as indicated. Note that the molar ratio of Cu to carrier equals 40/1; i.e., the highest carrier concentration applied was 125 nM (in panels G and I) which is below the LD_{50} values of all cell lines tested. The reduction of secreted Aβ40 (F and G) and Aβ42 (H and I) levels in treated APP-SH-SY5Y cell cultures is shown compared to the control. Treatment with free Cu ($p < 0.08$ at 0.31 μM Cu; $p < 0.0053$ at 1.25 μM Cu; $p < 0.004$ at 5 μM Cu) and Cu-loaded nanoparticles ($p < 0.0009$ at 1.25 μM Cu; $p < 0.0001$ at 5 μM Cu) led to a statistically significant decrease in Aβ42.

nonamyloidogenic APP pathway, thereby suppressing the formation of Aβ (*31*). Earlier studies in animals have reported that normalized or elevated Cu levels can inhibit or even remove AD-related pathological plaques and, thus, may confer desirable disease-modifying effects (*13*, *15*, *16*, *18*). In addition to beneficial effects that Cu has in AD pathogenesis, Cu also has effects in other diseases (*32*). There are an increasing number of reports on acquired Cu deficiency in adults, including those of an

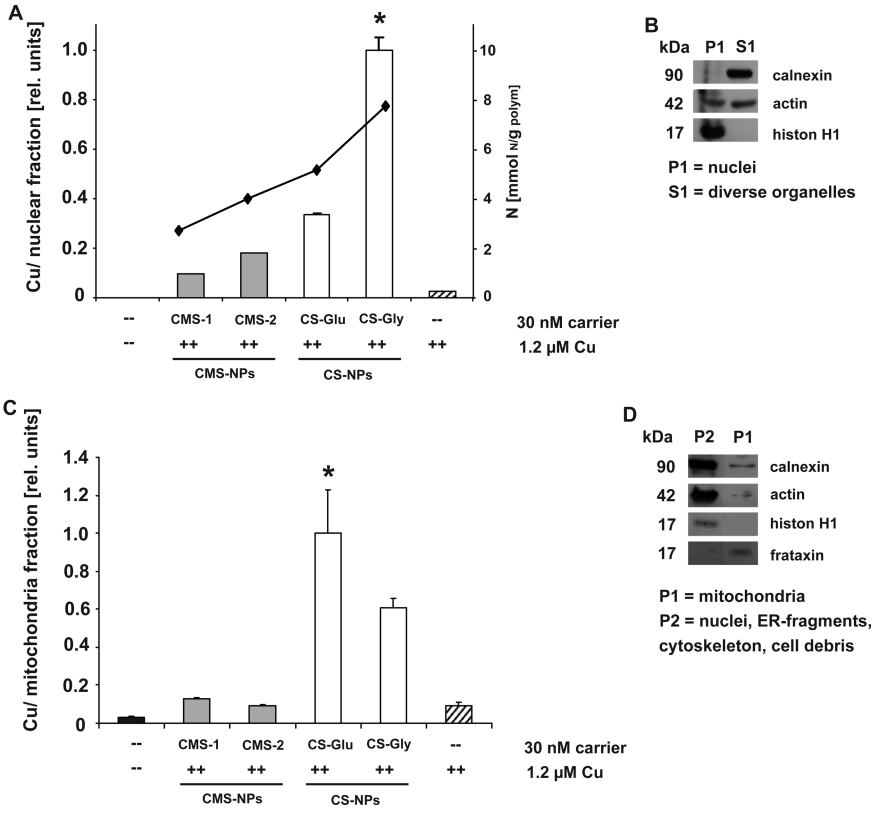

FIGURE 7: Cu-saturated CS nanoparticles specifically target nuclei and mitochondria. SH-SY5Y cells were cultured for 5 h in OptiMEM supplemented with 30 nM Cu nanoparticles charged with Cu. (A) Nuclei were isolated as described, and Cu content was determined by ICP-MS. CS-Gly specifically increased cellular Cu levels ($p < 0.0001$) compared to other carriers (white and gray bars). The target of intracellular transport is mainly determined by the terminal and linear amino groups of polymer [*N* (mmol/g of polymer)] (graph). (B) Analysis of nuclear fractions by the Western blot method. Total amounts of proteins standardized to 20 μg as measured by the BCA assay were separated on a 12% polyacrylamide−SDS gel, and organelle-specific marker proteins were detected by individual monoclonal antibodies as indicated. (C) Cu levels were measured by ICP-MS in mitochondrial fractions. CS-Glu specifically targeted mitochondria ($p < 0.0001$) compared to CMS carriers. (D) Analysis of mitochondrial fractions by Western blot analysis. Total amounts of proteins standardized to 20 μg as measured by the BCA assay were separated on a 12% polyacrylamide−SDS gel, and organelle-specific marker proteins were detected by individual monoclonal antibodies as indicated.

adult-onset Cu deficiency with neurological manifestations (*33*), an age-dependent breakdown of metal regulation as a consequence of aging (*34*), and an aberrant metal ion homeostasis as part of the AD pathogenic process (*13*, *15*, *16*, *18*).

In this study, we identified functionalized nanocarriers that bypass the Cu homeostatic system to therapeutically address the aberrant homeostasis implicated in AD pathogenesis (*13*). These carriers consist of PEI as the core molecule surrounded by one (CS-NPs) or two (CMS-NPs) organic shells, thereby shielding the Cu cargo from unwanted chemical reactions. Variants of these nanocontainers have already been tested for other purposes in clinical trials (*21*, *22*) focusing on their drug solubilization and delivery ability (*35*). They are specifically known to transport water-soluble drugs such as paclitaxel and other small organic anticancer molecules (*23*, *36*, *37*).

We have shown that higher supramolecular architectures of CS- and CMS-NPs (*24*) can encapsulate Cu ions and shield them from the environment during the transport to subcellular targets. Most likely, free amino groups at the core interact with Cu ions as guest molecules and bring these potential drugs into cells by bypassing the normal cellular uptake system. A recent clinical trial demonstrated that long-term intake of 8 mg of Cu-(II)-orotate-dihydrate can be excluded as a risk factor for AD based on CSF biomarker analysis (*17*), and directly affected levels of the diagnostic marker Aβ42. While the CSF Aβ42 level declined by 30% in the placebo group, it decreased by only 10% in the *verum* group (*17*). Although there were no Cu treatment effects on the cognitive performance of patients, results from studies in cell culture systems (*15*, *31*, *38*, *39*), dietary approaches with animal models for AD (*13*, *40*), and the clinical trial itself (*17*) indicate that Cu treatment has beneficial effects. Nevertheless, to reach the ultimate goal of an improved cognitive performance, Cu levels need to be increased in the brain and Cu ions must be made available for neuronal cells.

The carriers were tested for the following attributes: (i) to encapsulate Cu(II) but not other divalent metal ions tested, such as Zn(II) or Mn(II), and (ii) to increase bioavailability of Cu in yeast cells. Because we had verified Cu efflux activity of sAPP in yeast cells, we used this model as a test system for high-throughput analyses of nanocarriers. Two nanotransporters of the CMS-NP (CMS-1 and CMS-2) and two of the CS-NP candidates (CS-Glu and CS-Gly) were mainly selected for testing in higher eukaryotic cells due to their high specificity in encapsulating Cu ions. All four different carriers had a load maximum of ~40 copper ions per molecule. Thus, the Cu cargo of the nanotransporters was independent of the degree of functionalization (DF) (Table 1) but seemed to depend on the structure of the shell. Nanotransporters of the CMS-NP group could encapsulate slightly fewer Cu ions than CS-NPs, most likely due to the higher shielding of the core structure in the case of CMS-NPs.

We identified CS-NPs to increase intracellular Cu concentrations more efficiently than CMS-NPs. The activity of superoxide dismutase (SOD1) was tested as a reliable marker for bioavailable cytosolic Cu. According to the results, we conclude that the

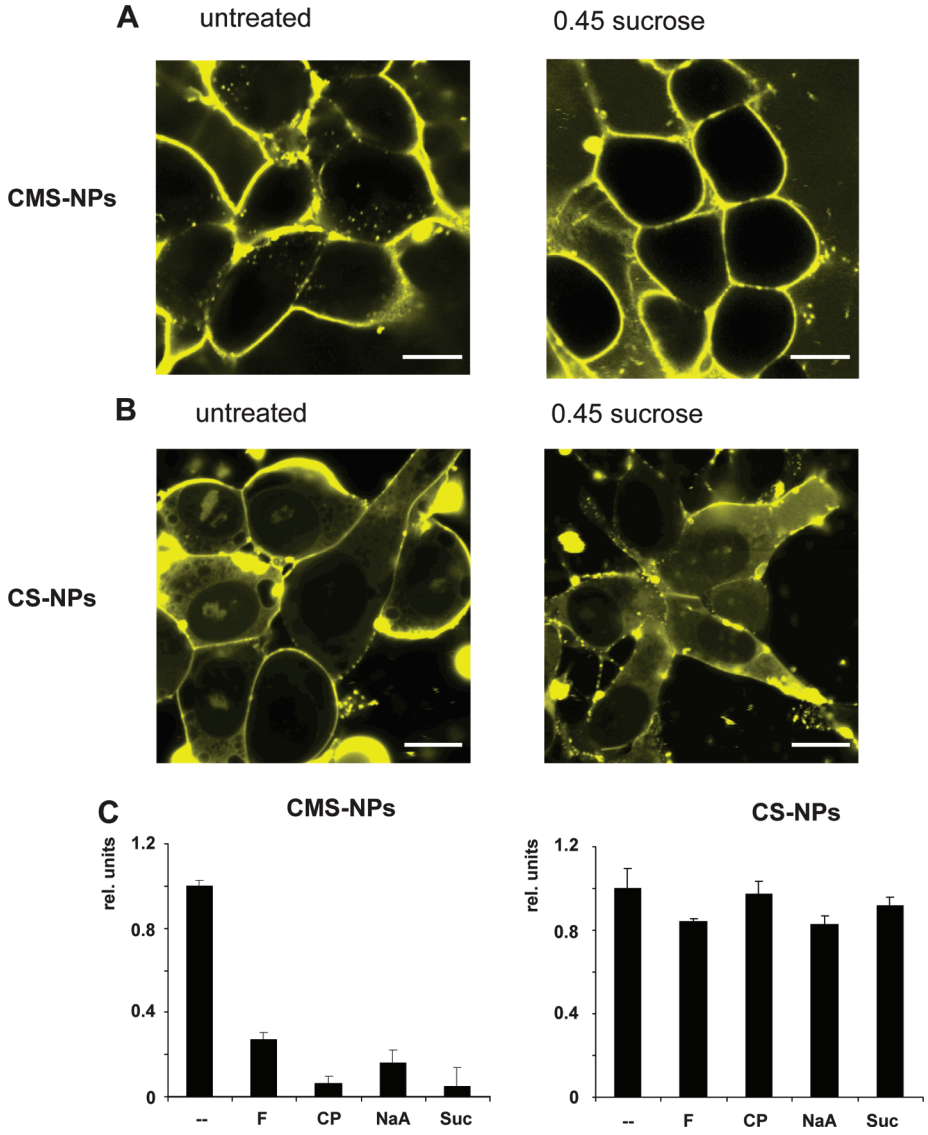

FIGURE 8: Mechanisms of cellular uptake of CMS-NP and CS-NPs. (A) Laser-scanning microscopy of SH-SY5Y cells revealed a vesicular staining of ICC-labeled CMS-NPs (left panel, control) that was not seen after preincubation in 0.45 M sucrose inducing hyperosmolarity (right panel). (B) Uptake of CS-NPs (left panel) was not inhibited by sucrose treatment (right panel). (C) Intracellular Cu levels as determined by ICP-MS that were preincubated with inhibitors for endocytosis. Cu levels were found reduced after treatment with CMS-NPs in the presence of inhibitors (left panel) but not for CS-NPs (right panel): F, filipin (0.7 μg/mL); CP, chlorpromazine (3.3 μg/mL); NaA, sodium azide (0.1%); Suc, sucrose (0.45 M). The scale bars in panels A and B are 10 μm.

excess Cu transported by nanocarriers is in an exchangeable form and is available for Cu-dependent enzymes such as SOD1 in the cytoplasm. Especially CMS-1 has released its bound guest molecules into the cytosol where it was available for the Cu-dependent enzyme SOD1. Therefore, CMS-1 and related structures may be highly suitable for antagonizing cytosolic Cu deficiency.

Cellular toxicity was measured in four higher eukaryotic cell lines, and this revealed that the shielding of the core structure by the surrounding shells determines the toxicity of the carriers. Under controlled nontoxic treatment conditions, intracellular Cu levels could be increased upon Cu-charged carrier treatment between 1.5-fold (CS-NPs) and 3-fold above normal (data not shown). This would equal 25% of the carrier-related LD_{50} and should be sufficient to rescue Cu depletion which has been observed in APP transgenic mice (*13*). Earlier attempts to address Cu depletion showed that the chelator clioquinol (CQ) could rescue it in vivo (*18*). CQ formed Cu complexes, which drastically increased the intracellular Cu concentration without affecting Zn levels in yeast cells (*15*). Clioquinol (CQ) or the derivatives PBT1 and PBT2 had shown promising results in animal models (*18*) and small clinical trials (*41*), and PBT2 was shown to have a positive effect on two executive function tests in phase II of a trial (*42*).

One of the main advantages of nanotransporters compared to other approaches is the possible controlled release of the cargo. So far, relatively little about how the encapsulated guest molecules from nanotransporters are released is known except that a pH-triggered cleavage of the shell can occur (*43*, *44*). In addition to the specific targeting of cellular compartments, redox-active Cu ions are protected like the Cu chaperones shielding Cu(I) from unwanted side reactions (*45*). Furthermore, CS-NPs transported almost 70% of the Cu cargo across intracellular membranes, whereas only half of the Cu load from CMS-NPs was found in intracellular organelles. This means that CS-NPs target intracellular organelles more efficiently than CMS-NPs that are localized more to the cytosol. Together with the easy release of the cargo, this may explain why CS-Glu but not other carriers

reduced the levels of secreted Aβ, which is mainly produced in endocytotic compartments (for a review, see ref *46*). Although the total increase in the cellular Cu level was greater after free Cu treatment, nanotransporters are superior to free Cu since they can target specific compartments, especially the CS-NPs. Our results indicate that CS-NPs can specifically target nuclei. The nuclear localization correlated with the cellular toxicity of CS-NPs and the nature of the surrounding shell. Thus, CMS-NPs may be the favored vehicles for providing enzymes with the essential cofactor Cu or for releasing Cu as a therapeutic agent similar to Isatin-Schiff base Cu(II) complexes that have been suggested for chemotherapeutic approaches (*19*, *47*, *48*).

Nanocarriers are internalized by cellular mechanisms distinct from those of other encapsulated reagents, e.g., those that are known as radiopharmaceutical drugs (*49*−*51*). The treatment with inhibitors indicated CMS-NP uptake occurs through a clathrin-mediated mechanism. Also, our study shows that a site-specific carrier delivery of hydrophilic cargo to certain cellular compartments is possible. We were able to show effects of cargo in living cells on enzyme activity and Aβ release and to unravel mechanisms of cellular uptake and intracellular redistribution of CMS-NPs and CS-NPs according to their chemical nature. Cu-charged nanocarriers offer the opportunity to bypass the cellular uptake systems, which is initially controlled by the Cu-mediated transport through Ctr1 (*52*, *53*). A risk assessment of long-term carrier treatment will be required for a possible treatment of metal ion deficiency disorders applying nanocarrier strategies. Especially for central nervous system-associated diseases, if and how nanocarriers can cross the blood−brain barrier and if the cargo is subsequently bioavailable, e.g., for neuronal cells, are questions that need to be investigated. Overall, nanocarriers hold real promise for delivering hydrophilic compounds such as Cu to particular tissues and may serve as therapeutic compounds in disorders associated with Cu deficiency.

ACKNOWLEDGMENT

We thank Thomas Wons, Gerhard Buchlow, and Andrea Senge for technical assistance and Johanna Dörsing for help with the figures.

REFERENCES

1. Pena, M. M., Lee, J., and Thiele, D. J. (1999) A delicate balance: Homeostatic control of copper uptake and distribution. *J. Nutr. 129*, 1251–1260.
2. Keen, C. L., Uriu-Hare, J. Y., Hawk, S. N., Jankowski, M. A., Daston, G. P., Kwik-Uribe, C. L., and Rucker, R. B. (1998) Effect of copper deficiency on prenatal development and pregnancy outcome. *Am. J. Clin. Nutr. 67*, 1003S–1011S.
3. Ponka, P. (2004) Hereditary causes of disturbed iron homeostasis in the central nervous system. *Ann. N.Y. Acad. Sci. 1012*, 267–281.
4. Waggoner, D. J., Bartnikas, T. B., and Gitlin, J. D. (1999) The role of copper in neurodegenerative disease. *Neurobiol. Dis. 6*, 221–230.
5. de Bie, P., Muller, P., Wijmenga, C., and Klomp, L. W. (2007) Molecular pathogenesis of Wilson and Menkes disease: Correlation of mutations with molecular defects and disease phenotypes. *J. Med. Genet. 44*, 673–688.
6. Bush, A. I., Pettingell, W. H., Multhaup, G., d Paradis, M., Vonsattel, J. P., Gusella, J. F., Beyreuther, K., Masters, C. L., and Tanzi, R. E. (1994) Rapid induction of Alzheimer Aβ amyloid formation by zinc. *Science 265*, 1464–1467.
7. Lovell, M. A., Robertson, J. D., Teesdale, W. J., Campbell, J. L., and Markesbery, W. R. (1998) Copper, iron and zinc in Alzheimer's disease senile plaques. *J. Neurol. Sci. 158*, 47–52.
8. Kang, J., Lemaire, H. G., Unterbeck, A., Salbaum, J. M., Masters, C. L., Grzeschik, K. H., Multhaup, G., Beyreuther, K., and Muller-Hill, B. (1987) The precursor of Alzheimer's disease amyloid A4 protein resembles a cell-surface receptor. *Nature 325*, 733–736.
9. Selkoe, D. J., Yamazaki, T., Citron, M., Podlisny, M. B., Koo, E. H., Teplow, D. B., and Haass, C. (1996) The role of APP processing and trafficking pathways in the formation of amyloid β-protein. *Ann. N. Y. Acad. Sci. 777*, 57–64.
10. Hesse, L., Beher, D., Masters, C. L., and Multhaup, G. (1994) The βA4 amyloid precursor protein binding to copper. *FEBS Lett. 349*, 109–116.
11. Multhaup, G., Schlicksupp, A., Hesse, L., Beher, D., Ruppert, T., Masters, C. L., and Beyreuther, K. (1996) The amyloid precursor protein of Alzheimer's disease in the reduction of copper(II) to copper (I). *Science 271*, 1406–1409.
12. White, A. R., Reyes, R., Mercer, J. F., Camakaris, J., Zheng, H., Bush, A. I., Multhaup, G., Beyreuther, K., Masters, C. L., and Cappai, R. (1999) Copper levels are increased in the cerebral cortex and liver of APP and APLP2 knockout mice. *Brain Res. 842*, 439–444.
13. Bayer, T. A., Schafer, S., Simons, A., Kemmling, A., Kamer, T., Tepest, R., Eckert, A., Schussel, K., Eikenberg, O., Sturchler-Pierrat, C., Abramowski, D., Staufenbiel, M., and Multhaup, G. (2003) Dietary Cu stabilizes brain superoxide dismutase 1 activity and reduces amyloid Aβ production in APP23 transgenic mice. *Proc. Natl. Acad. Sci. U.S.A. 100*, 14187–14192.
14. Bellingham, S. A., Lahiri, D. K., Maloney, B., La Fontaine, S., Multhaup, G., and Camakaris, J. (2004) Copper depletion down-regulates expression of the Alzheimer's disease amyloid-β precursor protein gene. *J. Biol. Chem. 279*, 20378–20386.
15. Treiber, C., Simons, A., Strauss, M., Hafner, M., Cappai, R., Bayer, T. A., and Multhaup, G. (2004) Clioquinol mediates copper uptake and counteracts copper efflux activities of the amyloid precursor protein of Alzheimer's disease. *J. Biol. Chem. 279*, 51958–51964.
16. Phinney, A. L., Drisaldi, B., Schmidt, S. D., Lugowski, S., Coronado, V., Liang, Y., Horne, P., Yang, J., Sekoulidis, J., Coomaraswamy, J., Chishti, M. A., Cox, D. W., Mathews, P. M., Nixon, R. A., Carlson, G. A., St George-Hyslop, P., and Westaway, D. (2003) In vivo reduction of amyloid-β by a mutant copper transporter. *Proc. Natl. Acad. Sci. U.S.A. 100*, 14193–14198.
17. Kessler, H., Bayer, T. A., Bach, D., Schneider-Axmann, T., Supprian, T., Herrmann, W., Haber, M., Multhaup, G., Falkai, P., and Pajonk, F. G. (2008) Intake of copper has no effect on cognition in patients with mild Alzheimer's disease: A pilot phase 2 clinical trial. *J. Neural Transm. 115*, 1181–1187.
18. Adlard, P. A., Cherny, R. A., Finkelstein, D. I., Gautier, E., Robb, E., Cortes, M., Volitakis, I., Liu, X., Smith, J. P., Perez, K., Laughton, K., Li, Q. X., Charman, S. A., Nicolazzo, J. A., Wilkins, S., Deleva, K., Lynch, T., Kok, G., Ritchie, C. W., Tanzi, R. E., Cappai, R., Masters, C. L., Barnham, K. J., and Bush, A. I. (2008) Rapid restoration of cognition in Alzheimer's transgenic mice with 8-hydroxy quinoline analogs is associated with decreased interstitial Aβ. *Neuron 59*, 43–55.
19. Filomeni, G., Cerchiaro, G., Da Costa Ferreira, A. M., De Martino, A., Pedersen, J. Z., Rotilio, G., and Ciriolo, M. R. (2007) Pro-apoptotic activity of novel Isatin-Schiff base copper(II) complexes depends on oxidative stress induction and organelle-selective damage. *J. Biol. Chem. 282*, 12010–12021.
20. Lee, J. Y., Friedman, J. E., Angel, I., Kozak, A., and Koh, J. Y. (2004) The lipophilic metal chelator DP-109 reduces amyloid pathology in brains of human β-amyloid precursor protein transgenic mice. *Neurobiol. Aging 25*, 1315–1321.
21. Matsumura, Y. (2006) [Micelle carrier system in clinical trial]. *Nippon Rinsho 64*, 316–321.
22. Nakanishi, T., Fukushima, S., Okamoto, K., Suzuki, M., Matsumura, Y., Yokoyama, M., Okano, T., Sakurai, Y., and Kataoka, K. (2001) Development of the polymer micelle carrier system for doxorubicin. *J. Controlled Release 74*, 295–302.
23. Duncan, R. (2006) Polymer conjugates for drug targeting. From inspired to inspiration!. *J. Drug Targeting 14*, 333–335.
24. Radowski, M. R., Shukla, A., von Berlepsch, H., Böttcher, C., Pickaert, G., Rehage, H., and Haag, R. (2007) Supramolecular aggregates of dendritic multishell architectures as universal nanocarriers. *Angew. Chem., Int. Ed. 46*, 1265–1269.
25. Krämer, M., Pérignon, N., Haag, R., Marty, J.-D., Thomann, R., Lauth-de Viguerie, N., and Mingotaud, C. (2005) Water-Soluble Dendritic Architectures with Carbohydrate Shells for the Templation and Stabilization of Catalytically Active Metal Nanoparticles. *Macromolecules 38*, 8308–8315.
26. Crooks, R. M., Zhao, M., Sun, L., Chechik, V., and Yeung, L. K. (2001) Dendrimer-encapsulated metal nanoparticles: Synthesis, characterization, and applications to catalysis. *Acc. Chem. Res. 34*, 181–190.
27. Simons, A., Ruppert, T., Schmidt, C., Schlicksupp, A., Pipkorn, R., Reed, J., Masters, C. L., White, A. R., Cappai, R., Beyreuther, K.,

Bayer, T. A., and Multhaup, G. (2002) Evidence for a copper-binding superfamily of the amyloid precursor protein. *Biochemistry 41*, 9310–9320.
28. Munter, L. M., Voigt, P., Harmeier, A., Kaden, D., Gottschalk, K. E., Weise, C., Pipkorn, R., Schaefer, M., Langosch, D., and Multhaup, G. (2007) GxxxG motifs within the amyloid precursor protein transmembrane sequence are critical for the etiology of Aβ42. *EMBO J. 26*, 1702–1712.
29. Wong, B. S., Pan, T., Liu, T., Li, R., Gambetti, P., and Sy, M. S. (2000) Differential contribution of superoxide dismutase activity by prion protein in vivo. *Biochem. Biophys. Res. Commun. 273*, 136–139.
30. Culotta, V. C., Yang, M., and O'Halloran, T. V. (2006) Activation of superoxide dismutases: Putting the metal to the pedal. *Biochim. Biophys. Acta 1763*, 747–758.
31. Borchardt, T., Camakaris, J., Cappai, R., Masters, C. L., Beyreuther, K., and Multhaup, G. (1999) Copper inhibits β-amyloid production and stimulates the non-amyloidogenic pathway of amyloid-precursor-protein secretion. *Biochem. J. 344*(Part 2), 461–467.
32. Zhao, G., and Lin, H. (2005) Metal complexes with aromatic N-containing ligands as potential agents in cancer treatment. *Curr. Med. Chem. Anticancer Agents 5*, 137–147.
33. Kumar, N. (2006) Copper deficiency myelopathy (human swayback). *Mayo Clin. Proc. 81*, 1371–1384.
34. Maynard, C. J., Bush, A. I., Masters, C. L., Cappai, R., and Li, Q. X. (2005) Metals and amyloid-β in Alzheimer's disease. *Int. J. Exp. Pathol. 86*, 147–159.
35. Duncan, R., and Izzo, L. (2005) Dendrimer biocompatibility and toxicity. *Adv. Drug Delivery Rev. 57*, 2215–2237.
36. Haag, R., Sunder, A., and Stumbé, J. F. (2000) An Approach to Glycerol Dendrimers and Pseudo-Dendritic Polyglycerols. *J. Am. Chem. Soc. 122*, 2954–2955.
37. Xu, S., Krämer, M., and Haag, R. (2006) pH-Responsive dendritic core-shell architectures as amphiphilic nanocarriers for polar drugs. *J. Drug Targeting 14*, 367–374.
38. Donnelly, P. S., Caragounis, A., Du, T., Laughton, K. M., Volitakis, I., Cherny, R. A., Sharples, R. A., Hill, A. F., Li, Q. X., Masters, C. L., Barnham, K. J., and White, A. R. (2008) Selective intracellular release of copper and zinc ions from bis(thiosemicarbazonato) complexes reduces levels of Alzheimer disease amyloid-β peptide. *J. Biol. Chem. 283*, 4568–4577.
39. White, A. R., Du, T., Laughton, K. M., Volitakis, I., Sharples, R. A., Xilinas, M. E., Hoke, D. E., Holsinger, R. M., Evin, G., Cherny, R. A., Hill, A. F., Barnham, K. J., Li, Q. X., Bush, A. I., and Masters, C. L. (2006) Degradation of the Alzheimer disease amyloid β-peptide by metal-dependent up-regulation of metalloprotease activity. *J. Biol. Chem. 281*, 17670–17680.
40. Maynard, C. J., Cappai, R., Volitakis, I., Cherny, R. A., White, A. R., Beyreuther, K., Masters, C. L., Bush, A. I., and Li, Q. X. (2002) Overexpression of Alzheimer's disease amyloid-β opposes the age-dependent elevations of brain copper and iron. *J. Biol. Chem. 277*, 44670–44676.
41. Ritchie, C. W., Bush, A. I., Mackinnon, A., Macfarlane, S., Mastwyk, M., MacGregor, L., Kiers, L., Cherny, R., Li, Q. X., Tammer, A., Carrington, D., Mavros, C., Volitakis, I., Xilinas, M., Ames, D., Davis, S., Beyreuther, K., Tanzi, R. E., and Masters, C. L. (2003) Metal-protein attenuation with iodochlorhydroxyquin (clioquinol) targeting Aβ amyloid deposition and toxicity in Alzheimer disease: A pilot phase 2 clinical trial. *Arch. Neurol. 60*, 1685–1691.
42. Lannfelt, L., Blennow, K., Zetterberg, H., Batsman, S., Ames, D., Harrison, J., Masters, C. L., Targum, S., Bush, A. I., Murdoch, R., Wilson, J., and Ritchie, C. W. (2008) Safety, efficacy, and biomarker findings of PBT2 in targeting Aβ as a modifying therapy for Alzheimer's disease: A phase IIa, double-blind, randomised, placebo-controlled trial. *Lancet Neurol. 7*, 779–786.
43. Jansen, J. F. G. A., Meijer, E. W., and de Brabander-van den Berg, E. M. M. (1995) The Dendritic Box: Shape-Selective Liberation of Encapsulated Guests. *J. Am. Chem. Soc. 117*, 4417–4418.
44. Krämer, M., Stumbe, J. F., Turk, H., Krause, S., Komp, A., Delineau, L., Prokhorova, S., Kautz, H., and Haag, R. (2002) pH-responsive molecular nanocarriers based on dendritic core-shell architectures. *Angew. Chem., Int. Ed. 41*, 4252–4256.
45. Prohaska, J. R., and Gybina, A. A. (2004) Intracellular copper transport in mammals. *J. Nutr. 134*, 1003–1006.
46. Thinakaran, G., and Koo, E. H. (2008) Amyloid precursor protein trafficking, processing, and function. *J. Biol. Chem. 283*, 29615–29619.
47. Chen, D., Peng, F., Cui, Q. C., Daniel, K. G., Orlu, S., Liu, J., and Dou, Q. P. (2005) Inhibition of prostate cancer cellular proteasome activity by a pyrrolidine dithiocarbamate-copper complex is associated with suppression of proliferation and induction of apoptosis. *Front. Biosci. 10*, 2932–2939.
48. Daniel, K. G., Gupta, P., Harbach, R. H., Guida, W. C., and Dou, Q. P. (2004) Organic copper complexes as a new class of proteasome inhibitors and apoptosis inducers in human cancer cells. *Biochem. Pharmacol. 67*, 1139–1151.
49. Dearling, J. L., Lewis, J. S., Mullen, G. E., Welch, M. J., and Blower, P. J. (2002) Copper bis(thiosemicarbazone) complexes as hypoxia imaging agents: Structure-activity relationships. *J. Biol. Inorg. Chem. 7*, 249–259.
50. Green, M. A., Klippenstein, D. L., and Tennison, J. R. (1988) Copper (II) bis(thiosemicarbazone) complexes as potential tracers for evaluation of cerebral and myocardial blood flow with PET. *J. Nucl. Med. 29*, 1549–1557.
51. Laforest, R., Dehdashti, F., Lewis, J. S., and Schwarz, S. W. (2005) Dosimetry of 60/61/62/64Cu-ATSM: A hypoxia imaging agent for PET. *Eur. J. Nucl. Med. Mol. Imaging 32*, 764–770.
52. Petris, M. J., Smith, K., Lee, J., and Thiele, D. J. (2003) Copper-stimulated endocytosis and degradation of the human copper transporter, hCtr1. *J. Biol. Chem. 278*, 9639–9646.
53. Puig, S., Lee, J., Lau, M., and Thiele, D. J. (2002) Biochemical and genetic analyses of yeast and human high affinity copper transporters suggest a conserved mechanism for copper uptake. *J. Biol. Chem. 277*, 26021–26030.
54. Quadir, M. A., Radowski, M. R., Kratz, F., Licha, K., Hauff, P., and Haag, R. (2008) Dendritic multishell architectures for drug and dye transport. *J. Controlled Release 132*, 289–294.